Available online at www.sciencedirect.com
ScienceDirect
International Journal of Pharmaceutics 351 (2008) 144–151
INTERNATIONAL JOURNAL OF PHARMACEUTICS
www.elsevier.com/locate/ijpharm

Polymorphism of linezolid: A combined single-crystal, powder diffraction and NMR study

Elisabetta Maccaroni [a,*], Enrica Alberti [a], Luciana Malpezzi [b,*], Norberto Masciocchi [a], Chiara Vladiskovic [c]

[a] *Dipartimento di Scienze Chimiche e Ambientali, Università dell'Insubria, Via Valleggio 11, I-22100 Como, Italy*
[b] *Dipartimento di Chimica, Politecnico di Milano, Via Mancinelli 7, I-20131 Milano, Italy*
[c] *Dipharma Francis S.r.l., Via Bissone 5, I-20021 Baranzate (MI), Italy*

Received 28 May 2007; received in revised form 18 September 2007; accepted 19 September 2007
Available online 29 September 2007

Abstract

Linezolid (*S*)-*N*-[[3-(3-fluoro-4-morpholinylphenyl)-2-oxo-5-oxazolidinyl]methyl] acetamide is one of the first commercially available (and most widely used) oxazolidinone antibiotics. It was selectively prepared as two anhydrous polymorphic forms, labelled form II and IV in accordance with preliminary reports in the patent literature. Form II has been characterized by single-crystal X-ray diffraction methods (orthorhombic, $P2_12_12_1$, $a = 6.536(1)$, $b = 9.949(1)$, $c = 24.807(3)$ Å, $V = 1613.1(3)$ Å^3, $Z = 4$, $Z' = 1$), while powders of form IV could be fully characterized by employing ab initio powder diffraction methods (triclinic, P1, $a = 6.5952(7)$ Å, $b = 10.9875(10)$ Å, $c = 12.9189(14)$ Å, $\alpha = 110.683(4)^\circ$, $\beta = 88.186(6)^\circ$, $\gamma = 105.826(6)^\circ$, $V = 840.5(2)$ Å^3, $Z = Z' = 2$). The interconversion of form II into form IV was studied by TG, DSC and thermodiffractometry, which indicated a quantitative (endothermic and irreversible) transformation (in air) just above 160 °C. On cooling from the melt, linezolid gives an oily material, stable at RT, which can be crystallized into form IV by controlled heating near 100 °C. These materials were further characterized by high-resolution ^{1}H and ^{13}C NMR studies, as well as by ^{13}C solid-state NMR.

Keywords: Linezolid; Crystal and molecular structure; Powder diffraction; Phase transition

1. Introduction

Linezolid (*S*)-*N*-[[3-(3-fluoro-4-morpholinylphenyl)-2-oxo-5-oxazolidinyl]methyl] acetamide was the first commercially available synthetic oxazolidinone antibiotic, firstly synthesized in 1996 (Brickner et al., 1996). The drug acts as antibacterial agent for the treatment of multidrug-resistant gram-positive bacterial infections. Specific applications are skin infections or nosocomial pneumonia, where other antibiotics such as methicillin or penicillin are not effective due to antibiotic resistance. Oxazolidinones exhibit their action through a mechanism that inhibits the bacterial protein synthesis at a very early stage, prior to chain initiation (Shinabarger et al., 1997; Swaney et al., 1998; Zhou et al., 2002; Colca et al., 2003).

Recently, it was discovered that solid linezolid could exist in different polymorphic forms. The linezolid form synthesized by Brickner et al., was originally defined as linezolid form I (Bergren, 2003) because its IR spectrum and melting point differ from those of form II. Successively, new forms of linezolid were claimed, form III (Mohan Rao and Krishna Reddy, 2005), IV (Aronhime et al., 2006a. WO 2006/004922) later shown to be identical to form III (Tenengauzer et al., 2007) and other hydrated or solvated crystalline forms (Aronhime et al., 2006b. WO 2006/110155). However, we easily noticed that form TIII is not a new polymorphic form of linezolid, but a mixture of forms II and IV; this is indeed in agreement with the observation that it is relatively easy to obtain linezolid form IV contaminated in different rates by form II (Tenengauzer et al., 2007).

Following our recent interests on the polymorphic behaviour of widely used pharmaceuticals (Fantin et al., 2003), and thanks to the newly developed ab initio XRPD structural techniques (David et al., 2002) employing conventional laboratory data only, we thought it would be possible to unravel the apparently

* Corresponding authors. Tel.: +39 031 326235; fax: +39 031 326320.
E-mail address: elisabetta.maccaroni@uninsubria.it (E. Maccaroni).

0378-5173/$ – see front matter © 2007 Elsevier B.V. All rights reserved.
doi:10.1016/j.ijpharm.2007.09.028

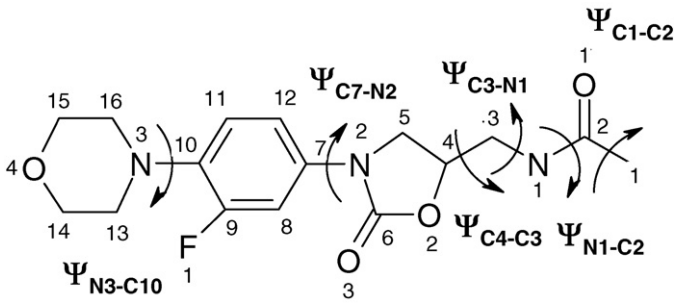

Scheme 1.

complex linezolid system by coupling diffraction data to thermal and spectroscopic (CPMAS) NMR analyses. In the following, we report the crystal structures and molecular stereochemistry of linezolid forms II and IV, as well as the complete characterization of their interconversion process.

In order to improve the legibility of this contribution, Scheme 1 reports a conventional drawing of the linezolid molecule, with the numbering scheme adopted in the following sections.

2. Experimental

2.1. Materials and methods

The two polymorphic forms of linezolid (forms II and IV) were synthesized according to the literature procedures reported in the patent US 6559305 (form II) and in the patent application US 2006/0142283 (form IV). Thermal analyses were performed using a Perkin-Elmer DSC-7 operated at the conditions of sample weight of few mg and a scanning rate of 10 °C/min. Elemental analyses were carried out on a Perkin-Elmer CHN Analyzer 2400 series II. ^{13}C and ^{1}H NMR measurements were performed on Bruker AVANCE 400 instrument. The spectra were obtained in $CDCl_3$ at 25 °C using tetramethylsilane (TMS) as indirect standard. For the solid-state NMR experiment a 4 mm double bearing MAS probe was employed. The ^{13}C CPMAS spectra were recorded using a recycle time of 60 s, contact time of 1 ms, spinning rate of 7 kHz at room temperature and transformed using a line broadening of 10 Hz.

2.2. Single-crystal X-ray structure analysis

Single-crystal X-ray measurements for linezolid form II were performed on a on a Siemens P4 diffractometer with graphite monochromated Cu Kα radiation (λ = 1.5418 Å), using the $\theta/2\theta$ scan technique. Unit cell parameters were determined using 51 reflections in the range $6.8 \leq 2\theta \leq 26.5°$; a total of 2912 reflections (2412 unique, $R_{int} = 0.054$) were collected, at room temperature, up to 130° in 2θ and index range: $-6 \leq h \leq 6$, $-11 \leq k \leq 11$, $-29 \leq l \leq 29$. No intensity decay was observed during data collection. The structure was solved by direct methods using SIR97 program (Altomare et al., 1999) and refined on F^2 by full-matrix least-squares procedure (Sheldrick, 1997), with anisotropic temperature factors for non-H atoms. H atoms, except H1N (which was freely refined with an individual isotropic temperature factor), were placed in geometrically calculated positions and refined in a riding model. The final refinement converged to $R = 0.048$ ($R_w = 0.124$) for 2165 observed reflections, with $I \geq 2\sigma(I)$, and $R = 0.055$ ($R_w = 0.130$) for all unique reflections. The goodness of fit, S, was 1.032. The final difference map showed a maximum and minimum residual peaks of 0.197 and 0.207e$^-$ Å^{-3}, respectively.

2.2.1. Crystal data

$C_{16}H_{20}FN_3O_4$; MW = 337.35 g mol^{-1}; $T = 293$ K; orthorhombic, space group $P2_12_12_1$; $a = 6.536(1)$ Å, $b = 9.949(1)$ Å, $c = 24.807(3)$ Å, $V = 1613.1(3)$ Å^3, $Z = 4$, $\rho_{calc} = 1.388$ g cm^{-3}, μ(Cu Kα) = 0.91 mm^{-1}; CCDC no. 648432.

2.3. Ab initio powder diffraction analysis

The XRPD pattern on the sample of linezolid form IV was collected on a Bruker D8 ADVANCE powder diffractometer operating in θ:θ mode, using Ni-filtered Cu Kα radiation (λ = 1.5418 Å) and a quartz monocrystal as a zero-background sample holder (supplied by *The Gem Dugout*, *PA*). Even if a capillary mounting is often used to minimize texture effects (Hill and Madsen, 2002), we found through the years that flat plate parafocussing geometry gives rather accurate diffraction data if a careful sample preparation is carried out. Needless to say, *in situ* thermodiffractometry is much easier if a flat sample mounting is used. The generator was operated at 40 kV and 40 mA, and diffraction data were recorded by a linear position-sensitive Lynxeye detector. Slits used: DS = 0.5°, AS 8 mm. A high-resolution scan was run from 5° to 85° 2θ, with step size of 0.02° and $t = 1430$ s step^{-1} (integrated over all PSD strips; total time: about 14 h).

Data were corrected for primary-beam contamination, removing the large background at low angles, and standard peak search methods employed to detect the first 20 well-defined lines in the diffraction pattern. Indexing by TOPAS (Coelho, 2003) of these peaks resulted in a triclinic lattice of ca. 840 Å^3. (GoF = 22.9) Density considerations suggested $Z = 2$ value. Given that the supplied material is enantiomerically pure, the space group assignment was obvious, as P1.

Instrumental parameters and lattice constants were optimized by a Le Bail refinement (Le Bail et al., 1992) using only the diffraction data below 40° 2θ. Structure solution was initiated by the simulating annealing technique implemented in TOPAS, (without intensity extraction) using two (crystallographically independent) molecular fragments derived from the (single-)crystal structure determination discussed above. Only the data below 40° 2θ were employed in this step. In P1, one molecule was kept fixed at the cell origin, while a number of rotations, translations and internal degrees of freedom (torsion angles) were adjusted to the best match between the measured and calculated powder diffraction pattern. The list of torsion angles freed during the simulation includes: H1-C1-C2-O1 (the methyl H-atoms orientation, with little impact on the calculated profile), O1-C2-N1-C3, C2-N1-C3-C4, H3-C3-C4-O2, C6-N2-C7-C8 and C9-C10-N3-C13 (for both independent molecules,

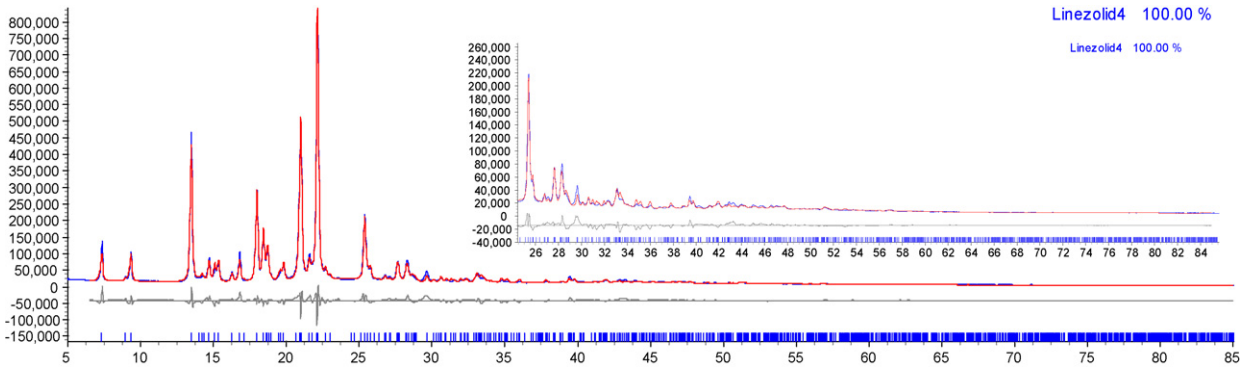

Fig. 1. Rietveld refinement plot for linezolid form IV, with peak markers and difference plot ($y_{obs} - y_{calc}$) at the bottom; blue: observed data (y_{obs}); red: calculated data (y_{calc}). The insert shows the 25°–85° 2θ at a magnified scale (3×).

see Scheme 1). The final Rietveld refinement (Rietveld, 1969) was eventually performed using a scale factor, a single isotropic thermal parameter, a preferred orientation correction, a polynomial description for the background contribution and a number of structural parameters including location and orientation of the molecular fragments and their torsion angles cited above. No antibump or distance restraints were introduced in the final refinement cycles, apart from the rigid body (with flexible torsion angles) definition reported above. Final R_w, R_p and R_{Bragg} values are: 0.101, 0.076 and 0.043 using all data up to 85° 2θ. The final Rietveld plot for this model is shown in Fig. 1.

2.3.1. Crystal data

$C_{16}H_{20}FN_3O_4$; MW = 337.35 g mol^{-1}; T = 293 K, triclinic, space group P1, a = 6.5952(7) Å, b = 10.9875(10) Å, c = 12.9189 (14) Å, α = 110.683(4)°, β = 88.186(6)°, γ = 105.826(6)°, V = 840.5(2) Å^3, Z = 2, ρ_{calc} = 1.333 g cm^{-3}, μ(Cu Kα) = 0.88 mm^{-1} CCDC no. 648433.

3. Results and discussion

3.1. Isolation of pure batches of linezolid form II and linezolid form IV

Form II was obtained by crystallization from ethyl acetate while polymorph IV was obtained starting from form II with hot slurry in toluene. The elemental analyses confirmed that the forms II and IV have exactly the same composition: $C_{16}H_{20}FN_3O_4$, calcd. C 56.97, H 5.97, N 12.46; found: (form II) C 56.87, H 5.91, N 12.35; (form IV) C 56.97, H 5.87, N 12.34.

3.2. Solid-state interconversions of linezolid forms II and IV

DSC measurements indicate that, when linezolid form II is heated up to 210 °C, a three-stage process (melt, recrystallization, melt) can be observed. As shown in Fig. 2, an endothermic process is observed around 155 °C (ΔH = 11.53 kJ mol^{-1}), immediately followed by an exothermic event at around 160 °C: accordingly, linezolid form II transforms into a new material (form IV, as confirmed by XRPD and TG analyses, the latter not showing any loss of mass below 180 °C) through a melt-recrystallization process (ΔH = −1.66 kJ mol^{-1}). Subsequently, a further endothermic event is observed around 180 °C, which can be attributed to melting of form IV, without decomposition (ΔH = 31.16 kJ mol^{-1}).

Apparently, form II can be transformed by heating to form IV through an endothermic process; in order to be energetically favoured, this transformation needs to be assisted by a significant increase in entropy, which, at higher T, counterparts the ΔH value by a negative $-T\Delta S$ contribution. The experimentally derived ΔH value, coupled to the estimate of the equilibrium temperature ($T \leq$ 155 °C) allows to determine the ΔS contribution as $\geq$27 J K^{-1} mol^{-1}, *i.e.* slightly higher than the typical values observed for (smaller) organic molecules (Gavezzotti and Flack, 2005). As shown later, form IV possesses a significantly larger molar volume (*i.e.* a lower density: 1.333 and 1.388 g cm^{-3} for forms IV and II, respectively) and a Z' = 2 structure (*i.e.* two crystallographically independent molecules with markedly different conformational values, *vide infra*). Both effects play a substantial role in increasing the entropy of this form (if compared to that of form II), mostly because a larger conformational freedom, and looser intermolecular contacts are present.

Moreover, a second DSC run was performed from 45 to 200 °C (with a scanning rate of 10 °C min^{-1}) on a material recovered from rapid cooling of molten linezolid; surprisingly,

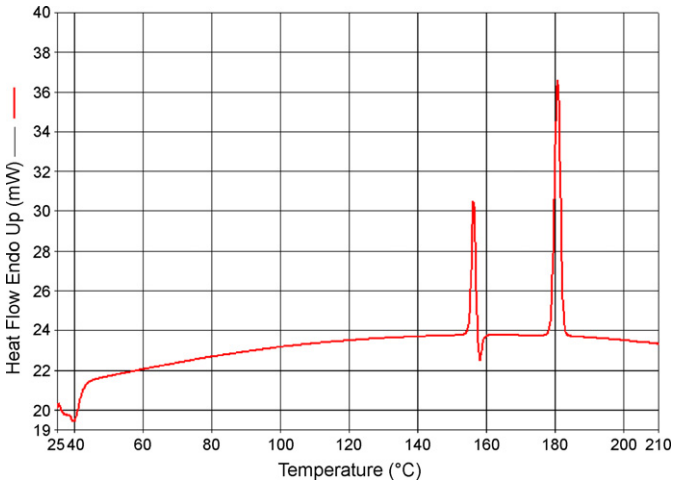

Fig. 2. DSC trace of linezolid form II.

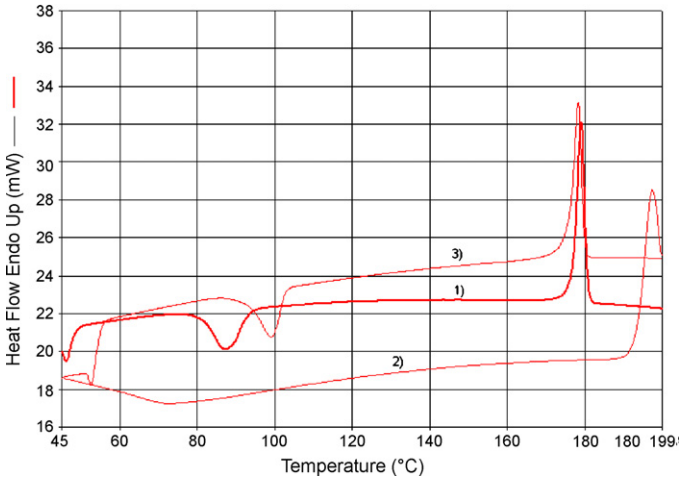

Fig. 3. DSC trace of amorphous (viscous) linezolid: (1) heating 10 °C min^{-1}; (2) cooling at 30 °C min^{-1} and (3) heating 10 °C min^{-1}.

this second trace (1 in Fig. 3) showed an exothermic (broad) peak ($\Delta H = 19.03$ kJ mol^{-1}) slightly above 80 °C and, as observed in the pristine measurement of linezolid form II (after transformation to form IV), a second event (melting) near 180 °C. These occurrences can be easily explained by the formation, upon cooling molten linezolid, of an amorphous material different from the known crystalline phases II and IV, which, near 80 °C regenerates form IV through recrystallization. In order to confirm this interpretation, we heated linezolid form IV above the melting point directly in the diffractometer chamber, and, upon cooling, we observed the formation of a viscous liquid, stable at RT. Gentle heating induced recrystallization to linezolid form IV (XRPD evidence) just above 90 °C. Fig. 3 shows two other curves: trace 2 refers to cooling molten linezolid at a controlled rate (−30 °C min^{-1}), while trace 3 relates to its subsequent heating (performed exactly as for trace 1). Evidently, the same events occur in 1 and 3, with a slight increase of the recrystallization temperature ($\Delta T = +10$ °C) for a "better organized" amorphous material obtained during the controlled cooling step.

3.3. NMR results

^{1}H and ^{13}C NMR data of linezolid in $CDCl_3$ solution were already reported in literature (Brickner et al., 1996; Yu and Huiyuan, 2002; Zhou et al., 2002; Mallesham et al., 2003; Madhusudhan et al., 2005) but to our knowledge, no assignment of the relative resonances of carbon atoms was ever cited. In Table 1 we propose the complete assignments of the carbon atom resonances and the values of the ^{13}C–^{19}F coupling constants derived combining 1D and 2D ^{1}H and ^{13}C NMR spectra obtained in $CDCl_3$ solution. In addition, Table 1 also contains the values of the ^{13}C chemical shifts observed for the two distinct polymorphic forms, form II and form IV, derived from the solid-state ^{13}C spectra shown in Fig. 4.

The ^{13}C CPMAS NMR spectra of linezolid show in general narrow peaks reflecting a high crystalline degree of the sample. It is interesting to observe that the C1 peak appears as a single narrow signal in form II whereas in form IV a splitting occurs.

Table 1
^{13}C chemical shifts (ppm) of linezolid in CD_3Cl solution and in solid-state (forms II and IV polymorphs)

Carbon number	Solution state δ (ppm)	Form II δ (ppm)	Form IV δ (ppm)
C1	23.5	23.4	**21.6**, **22.0**
C2	171.6	170.4, 169.9	171.2
C3	42.3	43.2	43.5
C4	72.4	73.1	73.1
C5	48.0	48.9 (*)	48.4
C6	154.8	154.9 (Broad)	–
C7	133.3 (d) $^{3}J_{CF} = 10$ Hz	133.7	133.7
C8	107.9 (d) $^{2}J_{CF} = 26.3$ Hz	109.2	106.4 (Broad)
C9	155.9 (d) $^{1}J_{CF} = 240$ Hz	157.2	154.9
C10	136.9 (d) $^{2}J_{CF} = 9.0$ Hz	138.4	136.6
C11	119.2 (d) $^{3}J_{CF} = 4.0$ Hz	119.5	117.9 (Broad)
C12	114.3 (d) $^{4}J_{CF} = 3.0$ Hz	118.5	113.7 (Broad)
C(13, 16)	51.4 (d) $^{4}J_{CF} = 3.0$ Hz	52.0 (Broad)	–
C(14, 15)	67.3	66.7 (Broad)	–

(*) Overlapping with spinning side bands.

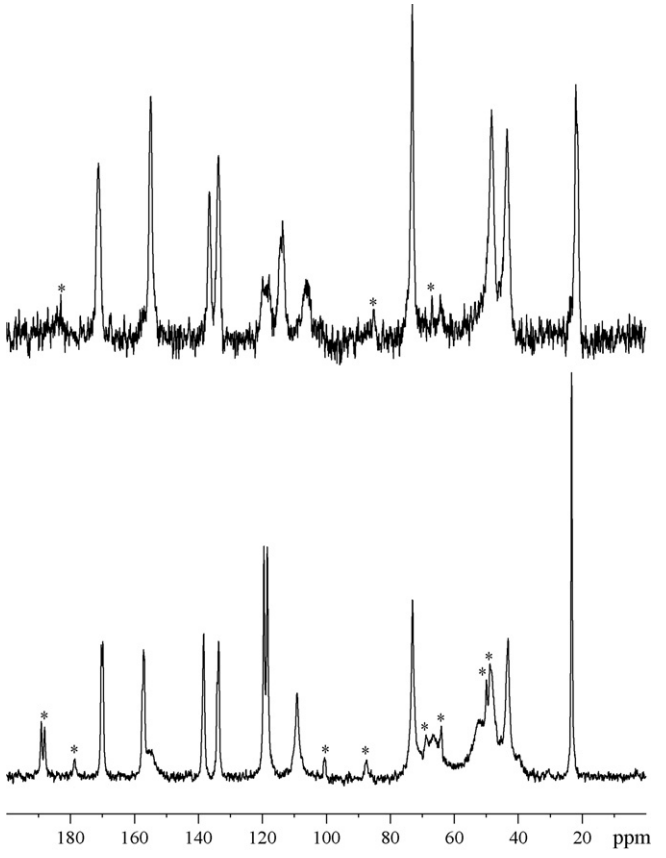

Fig. 4. ^{13}C CPMAS spectra of linezolid form II (bottom) and form IV (top). Asterisks indicate spinning side bands.

Table 2
Selection of the relevant conformational parameters of the two polymorphic forms of linezolid and of the unique analogue structure present in the Cambridge Structural Database, CCDC 214083, 5-((2,5-dioxopyrrolidin-1-yl)methyl)-*N*-phenyloxazolan-2-one

		Species			
		Linezolid form II	Linezolid form IV a	Linezolid form IV b	CCDC 214083
C9-C10-N3-C16°	$\Psi_{N3\text{-}C10}$	−68.8(4)	−167(1)	121(1)	n.a.
C8-C7-N2-C5°	$\Psi_{C7\text{-}N2}$	19.6(4)	−172(1)	177(1)	−18.6
O2-C4-C3-N1°	$\Psi_{C4\text{-}C3}$	−63.3(3)	−63(1)	−70(1)	−55.1
C4-C3-N1-C2°	$\Psi_{C3\text{-}N1}$	−89.4(4)	−104(1)	−142(1)	−87.5
C3-N1-C2-C1°	$\Psi_{N1\text{-}C2}$	180.0(3)	171(2)	174(2)	176.3
FO/morpholine conformation		*anti*/-*sc*	*syn*/-*ap*	*syn*/-*ac*	n.a.

Molecule: a, b.

This is in agreement with the crystallographic results indicating for form IV the presence of two independent molecules within the unit cell and only one for form II. For the remaining peaks in form IV a clear splitting of the signals is not evident, but the presence of two independent molecules generates a broadening of the signals.

The main chemical shift differences ($\Delta\delta$) between the two crystalline forms occur at the aromatic carbons (C8, C10, C11, C12) for which $\Delta\delta$ is about 1.6–4.8 ppm. This effect can be attributed to the different $\Psi_{N3\text{-}C10}$ and $\Psi_{C7\text{-}N2}$ torsion angles (Table 2) observed in the two forms; therefore, in the two polymorphs, different packing environments are present for the most rigid part of the molecule, while negligible modifications occur for the oxazolidine-amide branches, possibly thanks to their larger flexibility.

Worthy of note, a splitting of C2 in form II (170.4 and 169.9 ppm) is also evident. Since it was undoubtedly demonstrated that form II contains a crystallographically unique, and ordered, molecule, in order to explain the nature of this splitting, we tentatively attribute this effect to dipolar coupling to the quadrupolar ^{14}N nucleus, similarly to what already reported in literature (Frey and Opella, 1980; Hexem et al., 1981). Surprisingly, in the spectrum of form IV the signals relative to the resonances of C6, C13-C16 went unobserved. Due to their vicinity to nitrogen and oxygen atoms, these signals were already rather broad in the spectrum of form II. Probably, thanks to the splitting expected for the two independent molecules present in form IV, their intensity further decreases, vanishing in the noise of the spectrum.

3.4. Crystal and molecular structures of linezolid form II and linezolid form IV

Crystals of linezolid form II are orthorhombic, space group $P2_12_12_1$, and contain enantiomerically pure molecules packed by normal van der Waals forces and a few hydrogen

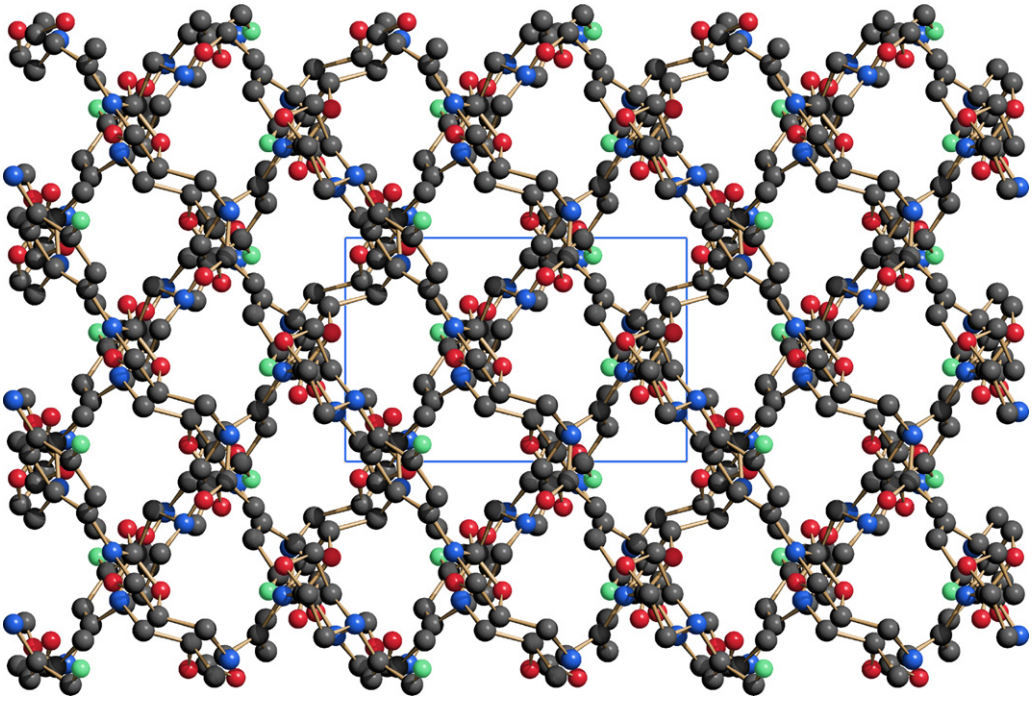

Fig. 5. Packing diagram (down [0 0 1]) of linezolid form II. Hydrogen atoms omitted for clarity.

bonds (N1···O3 2.99 Å): the latter connect symmetry related molecules winding up a 2_1 axis parallel to *b*, thus giving rise to monodimensional sequence of molecules of the catameric type. Obviously, other H···X contacts, stabilizing the crystal, are present, but the variety of their geometrical arrangement does not help in assigning clear-cut (energetically or structurally) relevant interactions. Viewed down *c*, the linezolid molecules, which can be idealized as a stretched sequence of three homo- and hetero-aromatic rings and of an acetamido branch, show their largest inertial axes packed almost normally one to each other (see Fig. 5).

Assuming substantial rigidity of the cyclic fragments, the conformation of the linezolid molecule can be meaningfully described by a few torsion angles, as shown in Scheme 1 above. With reference to Table 2, where the refined values of these torsion angles are reported, one can note the (expected) substantial planarity of the acetamido fragment, and the small value of the $\Psi_{C7\text{-}N2}$ angle (19.4°), the latter indicating that the F atom and the oxo fragment on the oxazoline ring point on opposite sides of the molecular ribbon. Fig. 6 (top) pictorially shows the whole molecule in its actual conformation as found in form II.

Differently, the structure of linezolid form IV was found to be triclinic (space group P1). The unit cell contains two independent molecules (hereafter labelled as molecules a and b), in agreement with the ^{13}C CPMAS NMR data. In this form, all molecules are nearly parallel (see the packing diagram shown in Fig. 7), but the two crystallographically independent molecules are oriented in a head-to-tail fashion (typically favoured by dipolar interactions); as in form II, they present intermolecular hydrogen bonds between the oxo(oxazoline) atoms and the amidic nitrogen atoms (in molecules a and b, respectively, 3.06 and 3.22 Å). Thus, noncentrosymmetric dimers are formed, through mutual coupling of molecules a and b across a pseudo symmetry element (a twofold axis running approximately parallel to [−1 1 1]).

That hydrogen-bonded molecules of pharmaceutical interest can afford significantly different packing topologies (*i.e.* dimers *vs.* chains) has already been demonstrated in the cases of dehydrocholic acid and Acitretin© (Fantin et al., 2003; Malpezzi et al., 2005), both studies having benefited from recently developed ab initio X-ray powder diffraction techniques.

The conformations of the two molecules (see Table 2) mainly differ at the $\Psi_{N3\text{-}C10}$ torsion angle, *i.e.* at the relative orientation of the swinging morpholine ring. This can be easily seen in Fig. 6 (bottom), where molecules a and b, with the fluoarene moiety isooriented in all drawings, are depicted. Indeed, since this angle refers to (differently substituted) sp^2 and sp^3 hybridized atoms, their rotational barrier is rather complex and, even in the gas phase, may present several distinct minima. However, also the other torsion angles show a (much more limited) variety: interestingly, if comparison is made with the molecular structure of 5-((2,5-dioxopyrrolidin-1-yl)methyl)-*N*-phenyloxazolan-2-one (Henkel, 2003), the only structural analogue of linezolid deposited in the CSD database, the latter closely matches the conformation found in form II (apart from a ca. 37° difference about the $\Psi_{C7\text{-}N2}$ torsion angle).

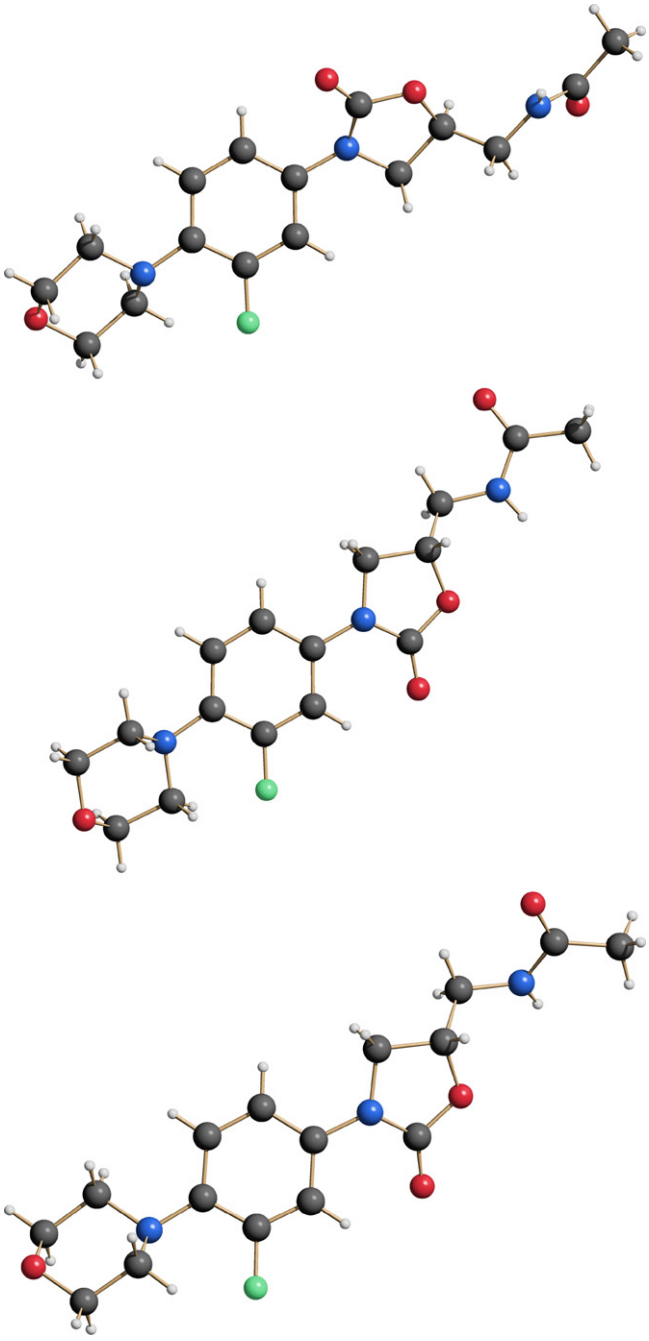

Fig. 6. Schematic drawing of the markedly different conformations of the linezolid molecule, as found in form II (top) and in the two crystallographically independent molecules of form IV (a and b). The fluoroarene moieties have been isooriented in all drawings.

The data reported in Table 2, and the above considerations can be usefully employed to address the relative stereochemistries of the linezolid molecules in forms II and IV; by defining the relative orientations of the F and oxo(oxazoline) atoms through a (FO) *syn–anti*-labelling scheme, and the morpholine torsion by conventional $\Psi_{N3\text{-}C10}$ *gauche-anti*-scheme, as reported in the last line of Table 2, where s = syn, c = clinal, a = anti, p = periplanar (IUPAC, 1976).

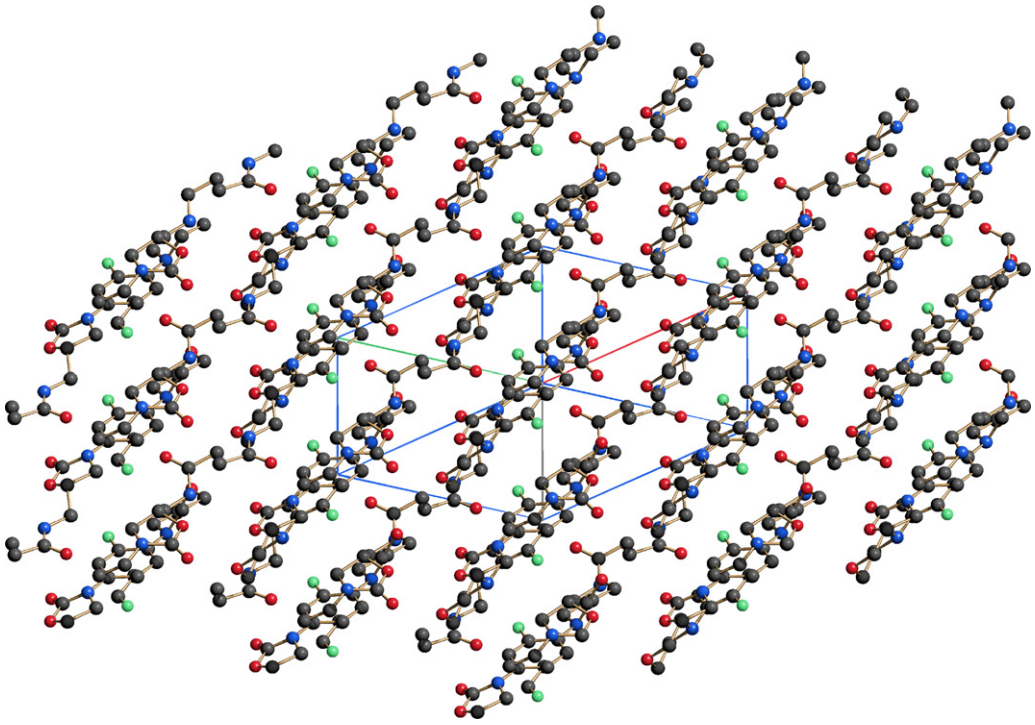

Fig. 7. Packing diagram (down [1 1 1]) of linezolid form IV, containing molecules (a and b, see text) arranged in a nearly parallel manner. Hydrogen atoms omitted for clarity.

3.5. Thermodiffractometry

The interpretation presented above for the DSC data was confirmed by XRPD patterns collected under different temperatures. In fact, the transformation from linezolid form II into form IV was followed directly in the diffractometer chamber using a custom made (Peltier driven) sample holder which allows to raise (and lower) the temperature, in air, in a very controlled manner (nominal 0.1 °C precision), up to (only) 150 °C. Progressive heating up to 150 °C showed that linezolid form II can be completely transformed into form IV. This is just slightly lower that the DSC transformation temperature, and suggests that this phase transition may also occur at lower temperature than originally observed, if enough time is allowed.

Worthy of note, the II → IV phase transformation does not occur through the formation of an (detectable) amorphous phase. Furthermore, this phase transition is clearly irreversible, leading to the formation of a stable polymorph, as already observed by Tenengauzer et al. (2007). In fact, form IV once formed, can be stored indefinitely (at RT), as a metastable phase; in addition, also a pressure-induced transformation (to the denser form II) was not detected after applying 1.2 GPa overnight to linezolid form IV in a hydraulic press. As expected, the only observable event in the XRPD spectrum was the peak broadening due to the formation of significantly smaller crystals.

4. Conclusions

The fortunate occurrence of single crystals of linezolid form II, the structure of which could be well determined using conventional diffraction methods, allowed the definition of an accurate molecular model to be subsequently employed in the powder diffraction study. Indeed, this latter method cannot afford atomic resolution, but in conjunction with ancillary observations (the single-crystal structure, analytical and spectroscopic evidences) can be positively used to derive, otherwise inaccessible, structural features. Accordingly, the crystal structure of linezolid form IV, available only as a polycrystalline material, was retrieved by state-of-the-art ab initio powder diffraction methods, which we (Masciocchi and Sironi, 2005), and others (David et al., 2002), have developed in recent years.

In the two forms studied here, three crystallographically independent molecules were characterized, the conformation of which could be analyzed by comparing the pertinent torsion angles. The most striking difference among them is the syn/anti-disposition of the fluoroarene residue with respect to the exocyclic oxygen of the oxazolidine ring and, to some extent, the supramolecular arrangement derived from weak hydrogen bonds, leading to catameric *vs.* dimeric assemblies, in forms II and IV, respectively. A complete picture of the interconversion process was derived by coupling conventional thermal analyses to thermodiffractometric measurements, allowing the determination of the energetics and kinetics of the II → IV → amorphous linezolid system.

Acknowledgements

Partial financial support from Fondazione CARIPLO. The authors are pleased to acknowledge the reviewers for valuable comments and suggestions, especially with respect to the XRPD data presentation.

References

Altomare, A., Burla, M.C., Camalli, M., Cascarano, G.L., Giacovazzo, C., Guagliardi, A., Moliterni, A.G.G., Polidori, G., Spagna, R., 1999. *SIR*97: a new tool for crystal structure determination and refinement. J. Appl. Cryst. 32, 115–119.

Aronhime, J., Koltai, T., Braude, V., Fine, S., Niddam, T., 2006. Crystalline form IV of linezolid. WO 2006/004922.

Aronhime, J., Koltai, T., Braude, V., Fine, S., Niddam, T., 2006. Solid Forms of Linezolid and Processes for Preparation thereof. WO 2006/110155.

Bergren, M.S., 2003. Linezolid-crystal form II. US6559305.

Brickner, S.J., Hutchinson, D.K., Barbachyn, M.R., Manninen, P.R., Ulanowicz, D.A., Garmon, S.A., Grega, K.C., Hendges, S.K., Toops, D.S., Ford, C.W., Zurenko, G.E., 1996. Synthesis and antibacterial activity of U-100592 and U-100766, two oxazolidinone antibacterial agents for the potential treatment of multidrug-resistant gram-positive bacterial infections. J. Med. Chem. 39, 673–679.

Coelho, A.A., 2003. TOPAS Version 3.1. Bruker AXS GmbH, Karlsruhe, Germany.

Colca, J.R., McDonald, W.G., Waldon, D.J., Thomasco, L.M., Gadwood, R.C., Lund, E.T., Cavey, G.S., Mathews, W.R., Adams, L.D., Cecil, E.T., Pearson, J.D., Boch, J.H., Mott, J.E., Shinabarger, D.L., Xiong, L., Mankin, A.S., 2003. Cross-linking in the living cell locates the site of action of oxazolidone antibiotics. J. Biol. Chem. 275, 21972–21979.

David, W.I.F., Shankland, K., McCusker, L.B., Baerlocher, C. (Eds.), 2002. Structure Determination from Powder Diffraction Data. Oxford Univ. Press, Oxford.

Fantin, G., Fogagnolo, M., Bortolini, O., Masciocchi, N., Galli, S., Sironi, A., 2003. Polymorphism of dehydrocholic acid: crystal structure of the β-phase and guest-mediated solid phase conversion. New J. Chem. 27, 1794.

Frey, M.H., Opella, S.J., 1980. High-resolution features of the ^{13}C NMR spectra of solid amino acids and peptides. J.C.S. Chem. Comm., 474–475.

Gavezzotti, A., Flack, H., 2005. Crystal Packing. In: Teaching Pamphlet. IUCr, Chester, UK.

Henkel, G., 2003. Data deposited with the Cambridge Structural Database as CCDC 214083.

Hexem, J.G., Frey, M.H., Opella, S.J., 1981. Influence of ^{14}N on ^{13}C NMR spectra of solids. J. Am. Chem. Soc. 103, 224–226.

Hill, R.L., Madsen, I.C., 2002. Sample preparation, instrument selection and data collection. In: David, W.I.F., Shankland, K., McCusker, L., Baerlocher, Ch. (Eds.), Structure Determination from Powder Diffraction Data, Chapter 6. Oxford University Press, Oxford, UK.

IUPAC, 1976. Commission on nomenclature of organic chemistry, section E: stereochemistry (recommendations 1974). Pure Appl. Chem. 45, 11–30.

Le Bail, A., Duroy, H., Fourquet, J.L., 1992. Crystal structure and thermolysis of $K_2(H_5O_2)Al_2F_9$. J. Solid State Chem. 98, 151–158.

Madhusudhan, G., Reddy, G.O., Ramanatham, J., Dubey, P.K., 2005. A novel and short convergent approach for *N*-aryl-5-aminomethyl-2-oxazolidinone derivatives linezolid and DUP-721. Ind. J. Chem. 44B, 1236–1238.

Mallesham, B., Rajesh, B.M., Reddy, P.R., Srinivas, D., Trenan, S., 2003. Highly efficient CuI-catalyzed coupling of aryl bromides with oxazolidinones using Buchwald's protocol: a short route to linezolid and toloxatone. Org. Lett. 5, 963–965.

Malpezzi, L., Grato, A.M., Masciocchi, N., Sironi, A., 2005. Single crystal and powder diffraction characterization of three polymorphic forms of Acitretin. J. Pharm. Sci. 94, 1067–1078.

Masciocchi, N., Sironi, A., 2005. Structural powder diffraction characterization of organometallic species: the role of complementary information. C.R. Chimie 8, 1617–1630.

Mohan Rao, D., Krishna Reddy, P., 2005. A novel crystalline for of linezolid. WO 2005/035530.

Rietveld, H.M., 1969. A profile refinement method for nuclear and magnetic structures. J. Appl. Cryst. 2, 65–71.

Sheldrick, G., 1997. SHELXL-97 Program for Crystal Structure Refinement. Gottingen, Germany.

Shinabarger, D.L., Marotti, K.R., Murray, R.W., Lin, A.H., Melchior, E.P., Swaney, S.M., Dunyak, D.S., Demyan, W.E., Buysse, J.M., 1997. Mechanism of action of oxazolidones: effects of linezolid and eperezolid on traslation reactions. Antimicrob. Agents Chemoter. 41, 2132–2136.

Swaney, S.M., Aoki, H., Ganoza, M.C., Shinabarger, D.L., 1998. The oxazolidone linezolid inhibits initiation of protein synthesis in bacteria. Antimicrob. Agents Chemoter. 42, 3251–3255.

Tenengauzer, R., Leibovici, M., Solomon, B-Z., 2007. Stable pharmaceutical composition comprising linezolid form IV. WO 2007/018588.

Yu, D., Huiyuan, G., 2002. Synthesis and antibacterial activity of linezolid analogues. Bioorg. Med. Chem. 12, 857–859.

Zhou, C.C., Swaney, S.M., Shinabarger, D.L., Stockman, B.J., 2002. H nuclear magnetic resonance study of oxazolidone binding to bacterial ribosomes. Antimicrob. Agents Chemoter. 46, 625–629.